Nanoscale

ROYAL SOCIETY
OF **CHEMISTRY**

PAPER
Guodong Meng *et al.*
A ferroelectrically modulated ultrasensitive two-dimensional
perovskite phototransistor with zero-gate-bias

NCNST

PAPER

Check for updates

A ferroelectrically modulated ultrasensitive two-dimensional perovskite phototransistor with zero-gate-bias†

Junyi She,[a] Hanlin Cen, [b] Zhiheng Shen,[a] Jianyu Wang,[a] Xin Liu,[a] Jun Xi, [b] Yonghong Cheng[a] and Guodong Meng *[a]

Two-dimensional (2D) organic–inorganic halide perovskites are promising sensitive materials for opto-electronic applications due to their strong light–matter interactions, layered structure, long carrier lifetime and diffusion length. However, a high gate bias is indispensable for perovskite-based phototransistors to optimize detection performances, since ion migration seriously screens the gate electric field and the deposition process introduces intrinsic defects, which induces severe leakages and large power dissipation. In this work, an ultrasensitive phototransistor based on the $(PEA)_2SnI_4$ perovskite and the $Al:HfO_2$ ferroelectric layer is meticulously studied, working without an external gate voltage. The nonvolatile remanent polarization provides a stable floating gate to locally define the potential profile, regulate barrier contact, and modulate carrier transport properties and charge redistributions, which facilitates an ultralow level of dark current and accurate photocurrent extraction at zero gate bias. Consequently, the fabricated phototransistor exhibits an outstanding responsivity and detectivity of 4918 A W^{-1} and 2.15 × 10^{15} Jones, respectively. The developed phototransistor contributes to advancements in optoelectronic applications including large-scale intelligent sensor arrays, light-wave communications and integrated circuits.

[a] State Key Laboratory of Electrical Insulation and Power Equipment, Xi'an Jiaotong University, Xi'an, 710049, China. E-mail: gdmengxjtu@xjtu.edu.cn
[b] School of Electronic Science and Engineering, Xi'an Jiaotong University, Xi'an, 710049, China
†Electronic supplementary information (ESI) available. See DOI: https://doi.org/10.1039/d4nr04910a

Guodong Meng is currently an associate professor at the State Key Laboratory of Electrical Engineering and Power Equipment in Xi'an Jiaotong University. He completed his Ph. D. in electrical engineering at Xi'an Jiaotong University. After graduation, he worked as a post-doctoral researcher at Massachusetts Institute of Technology, and then carried out research into two-dimensional materials and devices at the University of Oxford. His research interests include low-dimensional intelligent micro-sensors, state monitoring and diagnosis of power equipment, micro/nano discharge and plasma catalytic conversion.

Guodong Meng

Introduction

Two-dimensional (2D) layered perovskites with alternating organic and inorganic sheets such as $(C_6H_5C_2H_4NH_3)_2SnI_4$ $((PEA)_2SnI_4)$ have triggered significant attention for the exploration of high-performing optoelectronic devices such as photodetectors, solar cells and light emitting diodes, due to their appealing advantages of a high light absorption coefficient, direct bandgap, long exciton diffusion and carrier lifetime.[1–8] Furthermore, since the large organic spacing layer enables effectively depressing out-of-plane migration, 2D perovskites exhibit inhibited carrier scattering, efficient horizontal charge transport and improved ambient stability, which have great potential in promoting photodetection performances.

However, perovskite-based phototransistors require high-capacity gating since ion migration would screen the gate electric field. Several approaches have been attempted to enhance the gate modulation efficiency, such as introducing less-volatile inorganic cations, reducing the working temperature and decreasing the thickness of active materials.[9–13] Besides, solution treatment methods in the manufacturing process of perovskites result in structural disorder of grain boundaries, which impedes carrier transport and induces nonradiative recombination loss and a large dark current.[8,14–20]

Consequently, most of the phototransistors based on 2D perovskites are inevitably operating with a high gate bias to improve sensitivity at the cost of severe leakages and large power dissipation. Zhu *et al.* proposed a $(PEA)_2SnI_4$/semi-CNT hybrid phototransistor with an ultrahigh detectivity of 1.12×10^{17} Jones, which relied on a significant gate bias of 40 V to extract photocurrent.[21] Moreover, since the quantum barrier depth and thickness are dependent on the organic spacing layer, the realization of stable localized potential control still remains to be addressed. Further improvements have been demonstrated through interface engineering, adjusting the stoichiometric composition and introducing passivators to reduce defects in perovskites. However, it is still challenging to suppress the dark current while preserving decent responsivity and low power dissipation.

The use of ferroelectrics with switchable and nonvolatile remanent polarization, which are expected to serve as floating gates, locally defining the potential profile in semiconductors to modulate channel transport properties at zero gate bias, is a promising strategy.[9,22–29] Ferroelectric modulation provides benefits over other techniques for multipurpose photoelectric devices, namely accurate photocurrent extraction, inhibited power dissipation and tunable response wavelength. It has been reported that the ferroelectric-gated 2D phototransistor presented outstanding weak light detection ability under an illumination of 1.6 nW cm^{-2} (ref. 22) and extended response range from visible to near infrared (0.85–1.55 μm).[23] The method of ferroelectric local field modulation holds substantial potential in improving the detection efficiency and sensitivity.

In this work, we develop a gate-bias-free phototransistor based on the $(PEA)_2SnI_4$ perovskite and Al:HfO$_2$ ferroelectric film. The 2D perovskite layer is deposited for highly efficient light absorption, enhanced carrier transport, and optimized water and oxygen tolerance to promote the responsivity. The bottom ferroelectric layer is introduced to provide a localized electrostatic field improving gate control. Furthermore, the oriented ferroelectric domains enable charge redistributions, which could be used as a floating gate to regulate carrier transport properties, tune contact barriers, and depress dark current as well as ion migration without requiring a constant gate bias. The ferroelectric-gated phototransistor would break the trade-off between high detectivity and low noise power in a single system. At the same time, nonvolatile localized ferroelectric-gating could replace an external gate voltage, which significantly inhibits power consumption and heat loss.

Results and discussion

Structure and morphology

The preparation process of the proposed ferroelectric-gated phototransistor is shown in Fig. 1. The blade-coating method is used to synthesize the $(PEA)_2SnI_4$ perovskite on an Al:HfO$_2$ nanofilm, which is prepared by atomic layer deposition (ALD). The details of the device fabrication process are provided in the Experimental section. Optical microscopy is conducted to examine the morphology and surface properties of the proposed device. As shown in Fig. 2b, the resulted film is flat with satisfactory crystallinity. Furthermore, cross-sectional transmission electron microscopy (TEM) and energy-dispersive spectrometry (EDS) elemental mapping analysis are used to provide deeper insights into the good quality of the developed device. The sharp boundary contrast can be distinctly identified as shown in Fig. 2c, which demonstrates the clear and well-distributed presence of each functional layer. And the thickness of the Al:HfO$_2$/$(PEA)_2SnI_4$ layered structure is measured as 11.1/12.6 nm, respectively. Besides, the crystal structure of the prepared 2D perovskite is characterized through X-ray diffraction (XRD) as shown in Fig. 2d, where all patterns demonstrate typical regular peaks at $2\theta = 5.59°$, 10.95°, 16.38°, 21.88°, 27.39°, 33.04° and 38.66°, respectively, which are assigned to the ($00l$) (l = 2, 4, 6, 8, 10, 12 and 14) plane diffractions. The fabricated perovskite is confirmed to be oriented with the plane of alternating PEA$^+$ and $(SnI_4)^{2-}$ sheets parallel to the substrate surface, revealing the layered structure, which is promising in horizontal charge transport.[13,14] Furthermore, the optical properties of the deposited perovskite could be investigated using photoluminescence (PL) and ultraviolet-visible (UV-Vis) absorption spectra. The developed perovskite demonstrates a PL emission peak located at 632 nm with a narrow full width at half-maximum of 40 nm, which corresponds to the excitonic emission. Moreover, as shown in Fig. 2f, the prepared $(PEA)_2SnI_4$ film exhibits typical absorption peaks at 426, 522 and 612 nm. The characteristic peak at 426 nm corresponds to high exciton transition energy levels. The peak at 522 nm results from the charge transfer transition between organic and inorganic layers. And the latter narrow peak at 612 nm is attributed to intrinsic exciton absorption.[7,30] In addition, the ferroelectric characteristics of the Al:HfO$_2$ nanofilm are assessed from the hysteresis loop as shown in Fig. 2g. The coercive voltage and remanent polarization strength reach approximately 6.8 V and
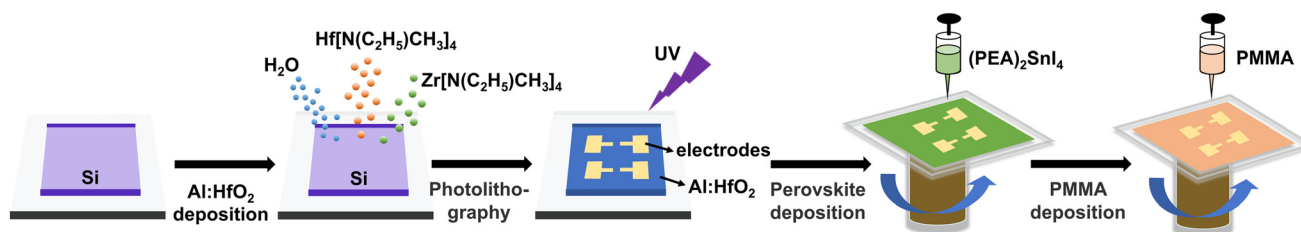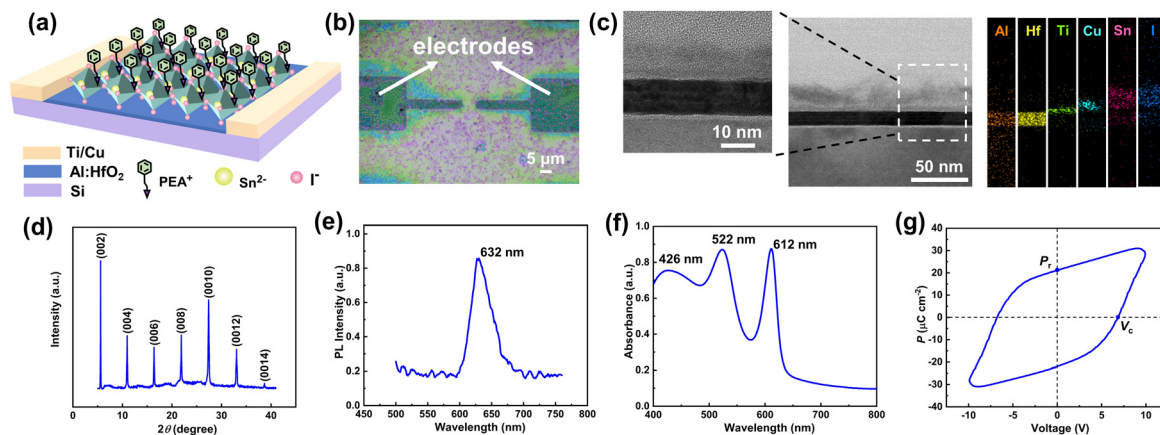

Fig. 1 Fabrication process of the proposed ferroelectric–gated 2D perovskite phototransistor.

Fig. 2 Characterization of the 2D perovskite phototransistor with ferroelectric-gating. (a) The schematic view of the device. (b) The optical microscopy of the as-fabricated phototransistor. (c) The cross-sectional transmission electron microscopy (TEM) image and energy-dispersive spectrometry (EDS) elemental mapping analysis of the developed phototransistor. (d) X-ray diffraction (XRD) pattern of the spin-coated perovskite. (e) Photoluminescence (PL) spectra of the 2D perovskite. (f) Ultraviolet−visible spectra of the deposited perovskite film. (g) Hysteresis loop of the fabricated Al:HfO$_2$ ferroelectric nanofilm; P_r and V_c represent remanent polarization and coercive voltage, respectively.

21.4 μC cm^{-2}, respectively, which enable a reservable and non-volatile localized field to modulate channel properties without requiring an external gate bias, indicating great potential in achieving low power dissipation and high level integration.

Polarizable and electrical modulation mechanisms of ferroelectric-gating

The polarizable and electrical modulation is implemented through a localized field induced by remanent polarization. Bipolar pluses with increasing amplitudes up to the coercive voltage of approximately 7 V at 1 kHz are applied at the gate electrode to enhance the coercive window, and then single pulses are triggered to strengthen the stability of polarization. Attributed to the thickness-dependent ferroelectricity, the Al:HfO$_2$ nanofilm contains decent polarization properties at the cost of low breakdown strength with the thickness of 11.1 nm. Hence, the gate voltage is determined to sweep ranging from 20 V to −20 V, which fully enables the gate's switching behaviors. As a result, a nonvolatile and reversable electric field over 10^8 V m^{-1} is introduced to regulate transport and contact properties, exhibiting as a clockwise hysteresis loop with an on/off ratio exceeding 10^6 shown in Fig. 3a. Since the current for backward sweep is higher than that for forward sweep in the transfer curve (I_{ds}−V_g), the ferroelectric polarization is confirmed to prevail the hysteretic mechanism rather than charge trapping. In addition, the voltage dependence of capacitance in the ferroelectric film is measured as shown in the inset of Fig. 3a. The permittivity of Al:HfO$_2$ is calculated to range from 10.5 to 11.9. Based on the slope of the transfer curve and the permittivity of the dielectric layer, the maximum value of the hole field-effect mobility reaches 1.61 cm^2 V^{-1} s^{-1}, according to the following formula:[31]

$$\mu = \frac{L}{W \times (\varepsilon_0 \varepsilon_r / d) \times V_{ds}} \times \frac{dI_{ds}}{dV_g} \quad (1)$$

where the channel length (L) and width (W) are measured as 5.8 and 4.3 μm, respectively, and the thickness of the Al:HfO$_2$ nanofilm (d) is 11.1 nm. The efficient charge transport contributes to the quantum confinement effect exerted by the large organic spacing layer, which limits the carrier transportation within the horizontal direction. Consequently, the fabricated device is promising in suppressing trapping and recombination of dissociated charges due to the inhibited carrier scattering, which facilitates a fast response speed and improved photodetection efficiency.

To further investigate the effect of Al:HfO$_2$ ferroelectric-gating on phototransistor performances, the output curves (I_{ds}−V_d) under the upward-polarization state (P$_{up}$), downward-polarization state (P$_{down}$) and without polarization state (Fresh) are obtained at zero gate voltage as shown in Fig. 3b. When the remanent polarization field is tuned to the P$_{up}$ state, the electrons are fixed at the interface between the perovskite and Al:HfO$_2$. And the channel transportation induced by dominated carriers of holes would be seriously disturbed by mobile cations. Simultaneously, the contact barrier between the perovskite and metal electrodes enlarges under the upward ferroelectric-gating, which significantly inhibits the conductance of the perovskite, leading to a depressed dark current down to the nanoampere range. Corresponding to the Kelvin probe force microscopy (KPFM) measurements, the surface potential of the perovskite on the ferroelectric film indicates an obvious decrease as the holes are depleted by the negative polarization charges on the top surface of Al:HfO$_2$ shown in Fig. S2,† which is consistent with the suppressed drain current. In contrast, the mobile cations would be attracted by the downward-oriented ferroelectric domains and bounded at the interface, resulting in large and stable flowing currents to occupy the channel. As a result, the accumulation of holes leads to an increase of surface potential as presented in Fig. S2.† At the same time, the contact barrier would decrease attributed to
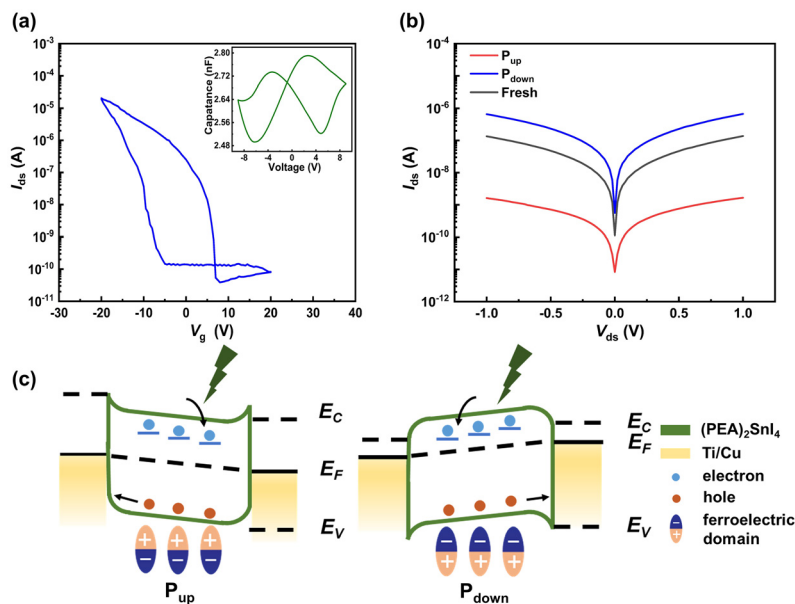
Fig. 3 Polarization-related electrical characterization of the proposed phototransistor. (a) Transfer curve (I_{ds}–V_g) of the fabricated device and the inset shows the voltage dependence of capacitance in Al:HfO$_2$ film. (b) The output curves (I_{ds}–V_{ds}) of the ferroelectric-gated phototransistor under Fresh (without polarization), P$_{up}$ (upward polarization) and P$_{down}$ (downward polarization) states. (c) The band diagrams of the perovskite and electrodes in P$_{up}$ and P$_{down}$ states. E_C, E_F and E_V represent the conduction band, Fermi level and valence band of the perovskite, respectively.

the downward energy band bending of the perovskite, which enables efficient tunneling of holes through the barrier. The working mechanisms and energy band diagrams of the ferroelectric-gated phototransistor are shown in Fig. 3c and 4. Moreover, a SiO$_2$-based phototransistor with the (PEA)$_2$SnI$_4$ channel is intentionally proposed to investigate the contribution of ferroelectric-gating. The transfer curve presents unhysteretic behavior and a restricted on/off ratio over 10^3, indicating a weak intrinsic switching effect on transport properties as shown in Fig. S3.† The significantly depressed off current for the Al:HfO$_2$-based device reveals that the introduced ferroelectric-gating plays a decisive role in modulating charge dynamics and weakening the Fermi level pinning effect, which enables improved photocurrent extraction. And it is especially promising for application in weak light detection.

Enhanced optoelectronic performances of the ferroelectric-gated 2D perovskite phototransistor

To better clarify the effect of ferroelectric-gating on improved optoelectronic performances, characterization of the proposed photodetector is performed in the P$_{up}$ state without an external gate voltage. Under light illumination at 530 nm wavelength, the output curves illustrate a linear and symmetry tendency as shown in Fig. 5a, which indicates the formation of quasi-Ohmic contacts regulated by the ferroelectric-induced nonvolatile electric field. Since charges are attracted by the oriented ferroelectric domains and fixed at the interface, employing as the floating gate, the fabricated device enables ultrasensitive and efficient extraction of the photocurrent from the depressed dark current, which is demonstrated as an outstanding on/off

ratio exceeding 10^7. To further evaluate the photoresponse properties of the ferroelectric-gated phototransistor, typical figures of merits such as responsivity (R) and detectivity (D^*) are measured. The responsivity is decided by the photocurrent over illumination light power, reaching the highest value of 4918 A W^{-1}, which is attributed to the high capacity gating. Besides, detectivity is calculated as $D^* = R(A\Delta f)^{1/2}/(I_S + I_T)$, where A is the photosensitive area, Δf is the bandwidth, I_S and I_T represent shot noise and thermal noise, respectively.[32,33] Owing to the high intrinsic carrier density and long carrier lifetime, the large dark current dominates the channel, which significantly weakens the photodetection capability, resulting in a suppressed detectivity of 8.8 × 10^{12} Jones in the Fresh state, as shown in Fig. S4.† Since the 2D perovskite with intense light-harvesting ability serves as an optimized light absorber, along with a ferroelectric-induced electrostatic field employed as a floating gate to efficiently inhibit noise current, the incident light signal could be accurately distinguished, leading to a remarkable detectivity of 2.15 × 10^{15} Jones in the P$_{up}$ state. As for the downward polarization state, the dark current is extremely improved to approximately microampere range and the photocurrent can be hardly extracted. Consequently, the detectivity is limited as 9.8 × 10^{11} Jones. Moreover, monolayer inorganic sheets sandwiched between long-chain organic layers of the 2D perovskite are used as quantum wells to prolong the carrier lifetime. Meanwhile, the oxygen vacancies introduced in the orthorhombic phase transition process of Al:HfO$_2$ would trap and deplete the generous charges of the perovskite at the interface through defect engineering, contributing to recirculation of photoexcited carriers
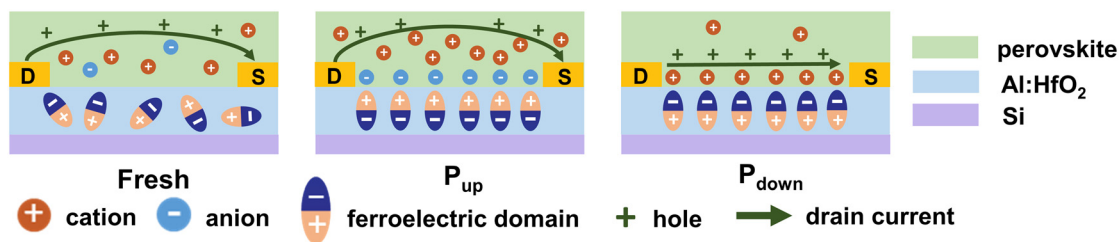
Fig. 4 The modulation mechanism of ferroelectric-gating for charge redistribution and ion mitigation in the perovskite phototransistor.
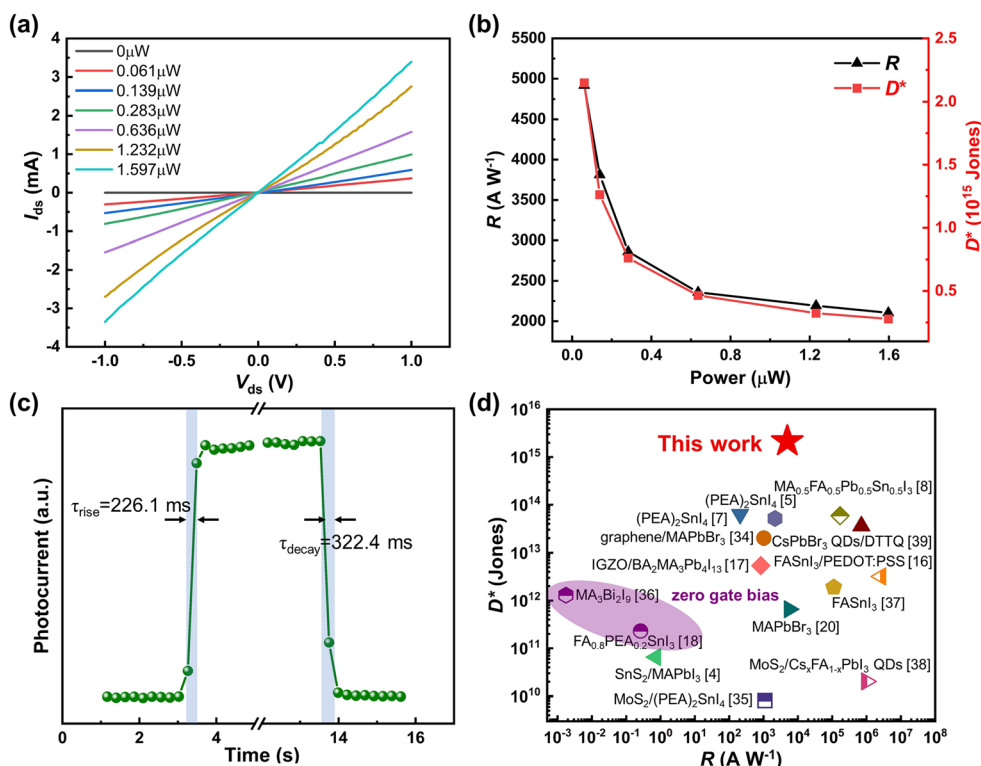

Fig. 5 Optoelectronic properties of the 2D perovskite phototransistor with ferroelectric-gating under the P_{up} state without a constant gate bias. (a) The output curves of the fabricated device under varied illumination powers. (b) The incident light power dependence of responsivity (R) and detectivity (D^*) at V_{ds} = 1 V. (c) The rise and decay times of the device. (d) The comparison of photoresponse performances corresponding to responsivity and detectivity between the proposed device and previously reported perovskite-based phototransistors. QDs, quantum dots; PEDOT:PSS, poly-(3,4-ethylenedioxythiophene):poly(styrenesulfonate); DTTQ, dithienothiophenoquinoid.

tunneling from drain to source before recombination. As a result, the fabricated phototransistor exhibits a prominent photogain (G) of 2.1×10^7 and an impressive external quantum efficiency (EQE) of 1.15×10^6%, respectively. Compared with the SiO$_2$-based device, the dark current is higher by orders of magnitude at a high gate voltage of 20 V, which introduces leakage paths and severe disorder. As a result, the ferroelectric-free phototransistor exhibits a poor detectivity of 2.3×10^{12} Jones as shown in Fig. S3,† which is attributed to the inefficient gate control through an external bias. In addition to the appealing photosensitivity, the time-resolved photoresponse of the ferroelectric-gated device is investigated as shown in Fig. 5c. The rise (τ_{rise}) and decay (τ_{decay}) times are estimated as

226.1 and 322.4 ms, respectively, due to the modulation of the long carrier lifetime that significantly boosts the photoelectric conversion efficiency *via* inhibited charge recombination at the cost of response speed.

A comparison between the proposed ferroelectric-gated phototransistor and previously reported perovskite-based devices is made to benchmark the photoresponse performances as shown in Fig. 5d,[4,5,7,8,16–18,20,34–39] which exhibits several characteristics: (i) An outstanding detectivity of up to 2.15×10^{15} Jones along with an impressive responsivity of 4918 A W^{-1} indicate superior overall optoelectronic performances compared with previous works, which demonstrates an accurate and highly efficient photocurrent extraction from the con-

siderably depressed noise current, especially in weak light detection. (ii) High-capacity ferroelectric-gating induced by nonvolatile remanent polarization provides a reversible and stable localized electrostatic field to modulate channel transport properties, charge redistributions and band alignments without requiring an external gate voltage, which contributes a significant reduction of power consumption compared with that of the reported devices working under a high gate bias up to −70 V.[8] (iii) An ultrathin dielectric layer at the sub-15 nm scale remarkably facilitates improved gating efficiency, high-levels of device integration and scalability as well as miniaturization.

Conclusions

In conclusion, we developed an ultrasensitive gate-bias-free phototransistor based on the highly photoactive 2D perovskite $(PEA)_2SnI_4$ and the functional ferroelectric nanofilm of Al:HfO_2. The polarized ferroelectric domains induced a nonvolatile and reversible localized field of up to 10^8 V m^{-1} through the electrostatic effect, which served as a floating gate to depress ion migration, define charge redistributions and regulate the contact barrier. Besides, the layered structure of the proposed device introduced defect engineering and inhibited carrier scattering, which was attributed to additional quantum wells and oxygen vacancies, considerably facilitating efficient charge transport and high gating efficiency. As a result, a prominent responsivity of 4918 A W^{-1} and a detectivity of 2.15×10^{15} Jones have been achieved at zero gate voltage, which are appealing values compared with those of previously reported devices working under high gate bias. The device's high capacity for polarizable nonvolatile ferroelectric-gating, sensitive photodetection capabilities and high scalability contribute to advancements in applications such as large-scale sensor arrays, flexible optoelectronics, solar cells, light-wave communications and imaging technology.

Experimental section

Material preparation

An Al:HfO_2 ferroelectric nanofilm with 8 mol% Al dopant concentration was prepared by atomic layer deposition (ALD) at 280 °C/20 Pa, where liquid tetrakis (diethylamide) hafnium (TDMAH), trimethyl aluminum (TMA) and O_2 plasma served as precursors for Hf, Al and oxygen, respectively. And then the films were processed through rapid thermal annealing (RTA) at 750 °C for 30 s to crystallize.

Device fabrication

The patterned source/drain electrodes of Ti/Cu were defined by standard ultraviolet lithography and thermally deposited through the lift-off process. For the blade-coating process, 2-phenylethylammonium iodide (PEAI) and SnI_2 were dissolved in dimethylacetamide (DMF) with a stoichiometric ratio of 2 : 1 to prepare precursor solutions, whose concentration was set to 0.2 mol L^{-1}. For film fabrication, 100 µL of the precursors was added dropwise onto Al:HfO_2 substrates with deposited electrodes, which have been modified by ultraviolet ozone surface treatment, and then spin-coated at 4000 rpm for 30 s. Afterwards, the coated films were annealed at 100 °C for 10 min to rapidly crystallize. To improve the stability in ambient air, the fabricated devices were spin-coated with polymethyl methacrylate (PMMA) at 2000 rpm for 60 s. After baking at 100 °C for 10 min, the encapsulated phototransistor based on the 2D perovskite and ferroelectric-gating were obtained. The microscopy image of the as-fabricated device under illumination is shown in Fig. S1.†

Characterization and measurements

The characterization of the morphology and crystallinity was performed by optical microscopy (OM, Olympus BX51-P), X-ray diffraction (XRD, Bruker, New D8 Advance), ultraviolet–visible spectrophotometry (Agilent, Cary 5000 UV-Vis-NIR), and photoluminescence spectroscopy (PL, Renishaw inVia confocal Raman system). The electrical and optical measurements were carried out at room temperature in ambient air using a semiconductor parameter analyzer (Keithley, Semiconductor Characterization System 4200A-SCS) equipped with a 530 nm laser diode.

Author contributions

G. M. and J. S. conceived the idea and designed the research. J. S. carried out most of the experimental work. X. L. helped with the deposition and dielectric measurements of Al:HfO_2. H. C. and J. X. assisted with the preparation of the perovskite. G. M., J. S., Z. S., J. W. and Y. C. wrote the manuscript with input from all the other authors. All authors were involved in extensive discussions and data analyses.

Data availability

Data for this article "A ferroelectrically modulated ultrasensitive two-dimensional perovskite phototransistor with zero-gate-bias", including the ferroelectric properties of remanent polarization in Al:HfO_2 nanofilm, such as the bipolar excitation method, field strength and switching persistence are available from ACS Publications at: **https://pubs.acs.org/doi/full/10.1021/acsami.3c15533**.

Conflicts of interest

The authors declare no competing interests.

Acknowledgements

References

1 C. Li, Y. Ma, Y. Xiao, L. Shen and L. Ding, *InfoMat*, 2020, **2**, 1247–1256.

2 Y. Zhang, Y. Ma, Y. Wang, X. Zhang, C. Zuo, L. Shen and L. Ding, *Adv. Mater.*, 2021, **33**, 2006691.

3 F. Cao and L. Li, *Adv. Funct. Mater.*, 2021, **31**, 2008275.

4 M. J. Loes, A. Lipatov, N. S. Vorobeva, H. Lu, J. Abourahma, D. S. Muratov, A. Gruverman and A. Sinitskii, *ACS Appl. Electron. Mater.*, 2023, **5**, 705–713.

5 J. Wu, Y. Miao, X. Qi, L. Yang, X. Wang, F. Zheng, F. Zhao, S. Shafique and Z. Hu, *ACS Photonics*, 2023, **10**, 4437–4446.

6 C.-K. Liu, H.-L. Loi, J. Cao, G. Tang, F. Liu, Q. Huang, X. Liang and F. Yan, *Small Struct.*, 2021, **2**, 2000084.

7 K. Yun, T. Lee, S. Kim, J. Kim and T. Seong, *Adv. Opt. Mater.*, 2023, **11**, 2201974.

8 H. Loi, J. Cao, C. Liu, Y. Xu, M. G. Li and F. Yan, *Small*, 2023, **19**, 2205976.

9 F. Wang, X. Zou, M. Xu, H. Wang, H. Wang, H. Guo, J. Guo, P. Wang, M. Peng, Z. Wang, Y. Wang, J. Miao, F. Chen, J. Wang, X. Chen, A. Pan, C. Shan, L. Liao and W. Hu, *Adv. Sci.*, 2021, **8**, 2100569.

10 Y. Wu, W. Chen, G. Chen, L. Liu, Z. He and R. Liu, *Nanomaterials*, 2018, **8**, 356.

11 G. Abiram, M. Thanihaichelvan, P. Ravirajan and D. Velauthapillai, *Nanomaterials*, 2022, **12**, 2396.

12 S. Li, X. Liu, H. Yang, H. Zhu and X. Fang, *Nat. Electron.*, 2024, **7**, 216–224.

13 F. Zhang, Q. Zhang, X. Liu, L. Qin, Z. Lou, Y. Hou and F. Teng, *J. Mater. Chem. A*, 2021, **9**, 22842–22853.

14 H. Zhu, A. Liu, T. Zou, H. Jung, S. Heo and Y.-Y. Noh, *Mater. Today Energy*, 2021, **21**, 100722.

15 X. Huang, Q. Li, W. Shi, K. Liu, Y. Zhang, Y. Liu, X. Wei, Z. Zhao, Y. Guo and Y. Liu, *Small*, 2021, **17**, 2102820.

16 C.-K. Liu, Q. Tai, N. Wang, G. Tang, Z. Hu and F. Yan, *ACS Appl. Mater. Interfaces*, 2020, **12**, 18769–18776.

17 T. Chen, C. Wang, G. Yang, Q. Lou, Q. Lin, S. Zhang and H. Zhou, *Adv. Mater. Technol.*, 2023, **8**, 2200679.

18 M. He, Z. Xu, C. Zhao, Y. Gao, K. Ke, N. Liu, X. Yao, F. Kang, Y. Shen, L. Lin and G. Wei, *Adv. Funct. Mater.*, 2023, **33**, 2300282.

19 Y. Ju, X. Wu, S. Huang, G. Dai, T. Song and H. Zhong, *Adv. Funct. Mater.*, 2022, **32**, 2108296.

20 H. Jing, R. Peng, R.-M. Ma, J. He, Y. Zhou, Z. Yang, C.-Y. Li, Y. Liu, X. Guo, Y. Zhu, D. Wang, J. Su, C. Sun, W. Bao and M. Wang, *Nano Lett.*, 2020, **20**, 7144–7151.

21 H. Zhu, A. Liu, H. L. Luque, H. Sun, D. Ji and Y.-Y. Noh, *ACS Nano*, 2019, **13**, 3971–3981.

22 T. Tong, Y. Gan, W. Li, W. Zhang, H. Song, H. Zhang, K. Liao, J. Deng, S. Li, Z. Xing, Y. Yu, Y. Tu, W. Wang, J. Chen, J. Zhou, X. Song, L. Zhang, X. Wang, S. Qin, Y. Shi, W. Huang and L. Wang, *ACS Nano*, 2023, **17**, 530–538.

23 X. D. Wang, P. Wang, J. Wang, W. D. Hu, X. H. Zhou, N. Guo, H. Huang, S. Sun, H. Shen, T. Lin, M. H. Tang, L. Liao, A. Q. Jiang, J. L. Sun, X. J. Meng, X. S. Chen, W. Lu and J. H. Chu, *Adv. Mater.*, 2015, **27**, 6575–6581.

24 Q. Chen, D. Lai, L. He, Y. Yan, E. Li, Y. Liu, H. Zeng, H. Chen and T. Guo, *ACS Appl. Mater. Interfaces*, 2021, **13**, 1035–1042.

25 B. Jeong, L. Veith, T. J. A. M. Smolders, M. J. Wolf and K. Asadi, *Adv. Mater.*, 2021, **33**, 2100486.

26 B. Jeong, P. Gkoupidenis and K. Asadi, *Adv. Mater.*, 2021, **33**, 2104034.

27 F. Cao, W. Tian, L. Meng, M. Wang and L. Li, *Adv. Funct. Mater.*, 2019, **29**, 1808415.

28 F. Li, C. Ma, H. Wang, W. Hu, W. Yu, A. D. Sheikh and T. Wu, *Nat. Commun.*, 2015, **6**, 8238.

29 J.-Y. Go, H. Zhu, Y. Reo, H. Kim, A. Liu and Y.-Y. Noh, *ACS Appl. Mater. Interfaces*, 2022, **14**, 9363–9367.

30 R. Li, C. Yi, R. Ge, W. Zou, L. Cheng, N. Wang, J. Wang and W. Huang, *Appl. Phys. Lett.*, 2016, **109**, 151101.

31 L. Q. Tu, R. Cao, X. D. Wang, Y. Chen, S. Q. Wu, F. Wang, Z. Wang, H. Shen, T. Lin, P. Zhou, X. J. Meng, W. D. Hu, Q. Liu, J. L. Wang, M. Liu and J. H. Chu, *Nat. Commun.*, 2020, **11**, 101.

32 Y. Chen, Y. Wang, Z. Wang, Y. Gu, Y. Ye, X. Chai, J. Ye, Y. Chen, R. Xie, Y. Zhou, Z. Hu, Q. Li, L. Zhang, F. Wang, P. Wang, J. Miao, J. Wang, X. Chen, W. Lu, P. Zhou and W. Hu, *Nat. Electron.*, 2021, **4**, 357–363.

33 C. R. Paul Inbaraj, R. J. Mathew, R. Sankar, H. Y. Lin, N.-X. Li, Y.-T. Chen and Y.-F. Chen, *ACS Appl. Mater. Interfaces*, 2023, **15**, 19121–19128.

34 Y. Zou, T. Zou, C. Zhao, B. Wang, J. Xing, Z. Yu, J. Cheng, W. Xin, J. Yang, W. Yu, H. Dong and C. Guo, *Small*, 2020, **16**, 2000733.

35 C. Fang, H. Wang, Z. Shen, H. Shen, S. Wang, J. Ma, J. Wang, H. Luo and D. Li, *ACS Appl. Mater. Interfaces*, 2019, **11**, 8419–8427.

36 A. A. Hussain, A. K. Rana and M. Ranjan, *Nanoscale*, 2019, **11**, 1217–1227.

37 C. Liu, Q. Tai, N. Wang, G. Tang, H. Loi and F. Yan, *Adv. Sci.*, 2019, **6**, 1900751.

38 S.-J. Jeong, S. Cho, B. Moon, J. A. Teku, M.-H. Jeong, S. Lee, Y. Kim and J.-S. Lee, *ACS Appl. Mater. Interfaces*, 2023, **15**, 5432–5438.

39 S.-H. Hong, S. N. Afraj, P.-Y. Huang, Y.-Z. Yeh, S.-H. Tung, M.-C. Chen and C.-L. Liu, *Nanoscale*, 2021, **13**, 20498–20507.